Egyptian Journal of Petroleum 28 (2019) 189–196

HOSTED BY

Contents lists available at ScienceDirect

Egyptian Journal of Petroleum

journal homepage: www.sciencedirect.com

Full Length Article

Anisotropy of permeability, P-wave velocity and electrical resistivity of Upper Cretaceous carbonate samples from Tushka Area, Western Desert, Egypt

Mohamed A. Kassab [a,*], Andreas Weller [b]

[a] Egyptian Petroleum Research Institute (EPRI), El Zohour Region, Naser City, Cairo, Egypt
[b] Institut für Geophysik, Technische Universität Clausthal, Arnold-Sommerfeld-Str. 1, 38678 Clausthal-Zellerfeld, Germany

ARTICLE INFO

Article history:
Received 26 August 2018
Revised 28 February 2019
Accepted 12 March 2019
Available online 21 March 2019

Keywords:
Carbonate rocks
Anisotropy
Permeability
Electrical resistivity
P-wave velocity
Tushka
Egypt

ABSTRACT

Petrophysical properties (such as porosity, permeability, grain density, bulk density, electrical resistivity, and P-wave velocity), as well as the anisotropy of the permeability, seismic velocity (P-wave velocity) and electrical resistivity were characterized in 42 carbonates (limestone) rock samples, collected from shallow wells (seven wells encountered the Upper Cretaceous carbonate rocks with variation in thickness, where well 1 encountered 50 ft thick Nubian sandstone, which decreased to about 30 ft thickness in well 7) from Tushka area, Egypt.

The petrographic investigation of the studied carbonate rock samples shows three microfacies associations: Facies1 (*MFA-1*) is mainly an oolitic, low dolomitic and low glauconitic, fossil-rich packstone with a tendency towards floatstone or rudstone, Facies 2 (*MFA-2*) is mainly a glauconite rich, low dolomitic floatstone with some tendencies towards rudstone and Facies3 *(MFA-3*) is mainly a sparry calcite-cemented, low dolomitic rudstone rich in glauconite and iron minerals.

The *MFA-2* with the lowest average density and highest average porosity is characterized by a strong anisotropy of both permeability and electrical resistivity. The values of the anisotropy ratio of seismic velocity (P-wave velocity) are close to one for all facies, this means that no anisotropy can be detected in the seismic velocity. A comparison between the coefficients of anisotropy reveals that the anisotropy of electrical resistivity and permeability are related to each other.

1. Introduction

The permeability of most sedimentary rocks indicates an anisotropic behavior with maximum permeability parallel to the plane of bedding. The permeability and the anisotropy of permeability depend on many factors, such as porosity, grain sorting and grain size distribution, cementation, clay content, and sedimentary fabric [20]. The complementary information on pore space, anisotropy, grain arrangement and their influences on elastic anisotropy, can be given by the incorporation of microstructural observations [11]. The fossil shape anisotropy and orientation is the main contributor to the anisotropy of both electric resistivity and permeability of highly fossiliferous limestones [15]. The anisotropy of permeability and seismic velocity is directly related to the anisotropy of the elastic rock frame, especially in the presence of fractures [4]. The anisotropy of permeability for sandstones is well correlated with the presence of bedding, while for volcanic rocks it is clearly related to the orientation of vesicles or cracks. However, no evident link between the geometry of the porous network and the permeability anisotropy appears for limestones probably because of the influence of the nonconnected porosity that does not contribute to the hydraulic transport [2].

Acoustic laboratory measurements have been conducted on clastic (sandstone) and non-clastic (limestone) rock samples to learn more about the behavior of acoustic wave velocities in clastic and non-clastic rock samples [7,8]. The elastic anisotropy is mainly controlled by the presence of an oriented system of open micro cracks, which may develop as a result of rock forming processes or tectonic deformation [12].

The seismic anisotropy is related to lithology, rock fabric and texture, and to its diagenetic history. So, that the analysis of seismic anisotropy provides an important tool for reservoir characterization and environmental and engineering applications [10].

Peer review under responsibility of Egyptian Petroleum Research Institute.
* Corresponding author.
E-mail address: mkassab68@yahoo.com (M.A. Kassab).

https://doi.org/10.1016/j.ejpe.2019.03.003
1110-0621/

The present study aims to throw light on petrophysical characterization of limestone rock samples of the Upper Cretaceous collected from Tushka Area, Egypt (Tushka area located at a latitude between 22°30′ and 22°45′N and longitude between 31°45′ and 32°00′E as shown in Fig. 1), with the main focus on the anisotropy of the permeability, electrical resistivity, and P-wave velocity. This part of the Tushka area is described as a flat topography with an elevated plateau to the north by the dissected plateau of Sinn El-Kaddab [19]. Issawi et al. (1969, 1999) established a more detailed formation division of Tushka area as follows:

Dungul Formation (Early Eocene) (Issawi et al., 1969) [6]
Garra Formation (Late Paleocene – Early Miocene)
Kurkur Formation (Early Paleocene)
Dakhla Formation (Maastrichtian)
Nubia Formation (Upper Cretaceous) (Issawi et al., 1999) [26]
Cenomanian Burg Formation (Cretaceous)
Abu Ballas Formation (Jurassic – Late Cretaceous)
Abu Simbel Formation (Jurassic)
Gilf Formation (Carboniferous)
Pre-Cambrian rocks (base)

2. Sampling and methods

The petrographic studies are based on the investigation of 17 thin sections that were prepared using vacuum impregnation with blue epoxy. The microscopy proved to be useful in the recognition of both porosity types and mineral composition of the rock matrix and cement. The petrophysical measurements were conducted on 42 carbonate samples (26 samples represent *MFA-1*, while 8 samples represent *MFA-2*, and 8 samples represent *MFA-3*).

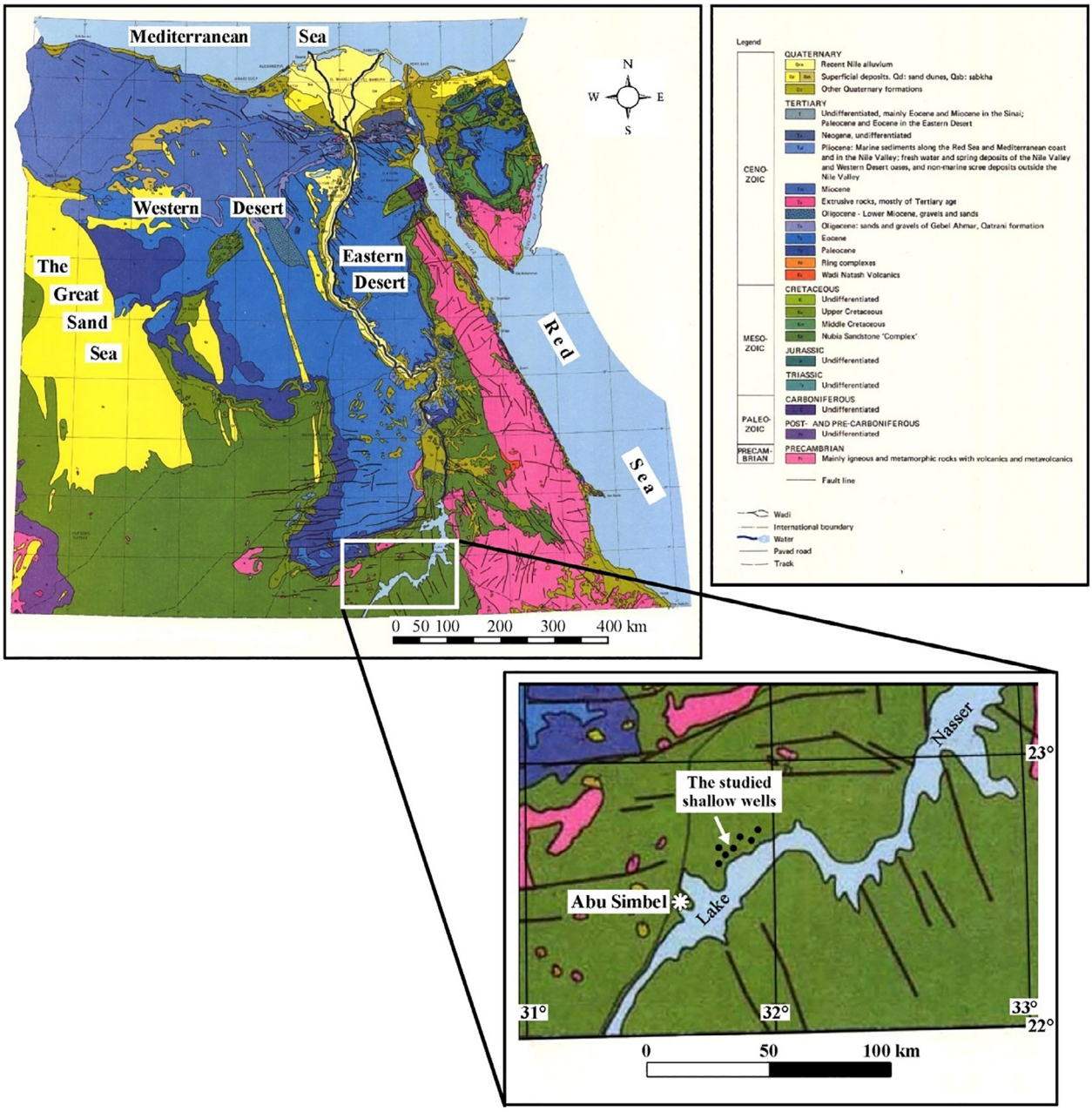

Fig. 1. Geological map of Egypt (modified after Said, 1962 [19]) indicating the location of the study area.

The samples were prepared in two directions (parallel and perpendicular to the bedding planes) by cutting cylindrical core plugs with a diameter of about 2.5 cm and a length of up to 3.5 cm. The samples were cleaned using soxhlet extraction. Toluene was used to remove any residual hydrocarbons, and methanol was used to remove residual salts.

The laboratory measurements of petrophysical parameters (porosity, permeability, and bulk and grain density) were performed under ambient conditions after drying of the samples. An electronic balance provided the mass of the dry and fully water saturated samples. An additional weighting of the immersed sample and using the Archimedes' principle yields the volume of the sample in cm^3. The bulk density ($\boldsymbol{\sigma}_b$) of rock samples was calculated from the ratio between the dry mass (m_d) and the bulk volume of the sample (V_b):

$$\boldsymbol{\sigma}_b = m_d / V_b \tag{1}$$

The grain density ($\boldsymbol{\sigma}_g$) was determined by the ratio between dry mass and the volume of the solid constituents of the rock or volume of rock grains (V_g):

$$\boldsymbol{\sigma}_g = m_d / V_g \tag{2}$$

V_g is determined by a matrix cup helium porosimeter (Heise Gauge type) for grain volume estimation and it can be determined from the difference between the bulk volume of the sample V_b and the volume of the pore space V_p:

$$V_g = V_b - V_p \tag{3}$$

The pore volume V_p is determined from the difference between the bulk volume of the sample and the grain volume. Porosity (ϕ) is defined as the ratio of the volume of void or pore space V_p to the bulk volume V of the rock sample:

$$\phi = \frac{V_p}{V_b} \tag{4}$$

The gas permeability (k) has been determined by a steady state permeameter. The electrical resistivity ($\boldsymbol{\rho}_o$) was measured using the resistivity meter model Gen Rad 1689 MRLC Digibridge and a Hassler type core holder with two copper electrodes for cylindrical core samples fully saturated with sodium chloride solution at 60000 ppm. This brine solution concentration results in a water resistivity $\boldsymbol{\rho}_{w3} = 0.116\ \Omega m$. The formation resistivity factor (F) according to Archie (1942) [1] is defined as the ratio between the resistivity of a fully saturated porous rock ($\boldsymbol{\rho_0}$) and the resistivity of the electrolyte ($\boldsymbol{\rho}_w$):

$$F = \frac{\rho_o}{\rho_w} \tag{5}$$

The relation between both formation resistivity factor (F) and porosity can be described by the following equation (1stArchie equation):

$$F = \frac{a}{\phi^m} \tag{6}$$

The compressional wave velocity (P-wave velocity, v_p) of the full water saturated samples were measured by an equipment of Inspection Technologies (USLT 2000) at ultrasonic frequencies of about 1 MHz, at room temperature and ambient pressure. The velocity of the samples is related to its elastic coefficients, internal structure, and density.

A material is anisotropic if the value of the directional petrophysical parameters of a rock property (e.g. permeability, electrical resistivity and P-wave velocity) varies with orientation of the samples (parallel to the bedding plane in the horizontal direction while the other is perpendicular to bedding plane in the vertical direction). Anisotropy of permeability (A_k) could be expressed by several formulas. A simple approach, [21,22] considers the quotient of horizontal or longitudinal permeability ($k_H = k_l$) and vertical or transversal permeability ($k_V = k_t$):

$$A_k^* = \frac{k_l}{k_t} = \frac{k_H}{k_V} \tag{7}$$

Halisch et al. (2009) [5], proposed another coefficient of anisotropy of permeability that enables better comparability of electrical and hydraulic anisotropy:

$$A_k = \sqrt[4]{k_l / k_t} \tag{8}$$

Serra (1988) [25] referred to the importance of measuring electric resistivity in two directions; the first is parallel to the bedding plane in the horizontal direction ($\rho_H = \rho_l$) while the other is perpendicular to bedding plane in the vertical direction ($\rho_V = \rho_t$) to calculate electric anisotropy (A_ρ). In the case of saturation with high salinity brine, the influence of surface conductivity can be ignored [18], so that in this study the resistivity at saturation with high salinity brine will be considered. In the case of anisotropic samples, the resistivity depends on the direction of current flow. According to a definition given by Keller and Frischknecht (1966) [9], the coefficient of anisotropy (A_ρ) is determined by taking the square root of the ratio of resistivity measured in the two principal directions, across the bedding planes (vertical or transversal resistivity $\rho_v = \rho_t$) and along the bedding planes (horizontal or longitudinal resistivity $\rho_H = \rho_l$):

$$A_\rho = \sqrt{\frac{\rho_t}{\rho_l} = \frac{\rho_V}{\rho_H}} \tag{9}$$

Since for layered structures the transversal resistivity in general, exceeds the longitudinal resistivity, the coefficient of anisotropy A_ρ can be assumed to be larger than one. The longitudinal resistivity results from the measurement at the horizontal sample and the transversal resistivity from the vertical sample. A seismic anisotropy ratio is defined using the measured velocity values parallel (v_{pH}) and perpendicular (v_{pV}) to the stratification [20]:

$$AV = v_{PH} / v_{PV} \tag{10}$$

The determined petrophysical parameters, the anisotropy of permeability, the anisotropy of electrical resistivity, and the anisotropy of P-wave velocity (Minimum, maximum and average values) are compiled in Tables 1–4.

3. Results and discussion

3.1. Petrographic investigations

Regarding the investigation of the thin sections, the studied rock samples can be divided into three facies, which can be described according to Dunham (1962) [27] as Facies1 (*MFA-1*) is mainly an oolitic, low dolomitic and low glauconitic, fossil-rich packstone with a tendency towards floatstone or rudstone (Fig. 2A–D), Facies 2 (*MFA-2*) is mainly a glauconite rich, low dolomitic floatstone with some tendencies towards rudstone (Fig. 2E–H), and Facies3 (*MFA-3*) is mainly a sparry calcite cemented, low dolomitic rudstone rich in glauconite and iron minerals (Fig. 2I–L).

The petrographic investigation is focused on the texture and composition of the analyzed samples. The three microfacies associations [Facies1 (*MFA-1*), Facies 2 (*MFA-2*) and Facies 3 (*MFA-3*)] were characterized in former studies by El Sayed et al., (2005) [3] and Öner (2014) [17].

There is mainly radial cementation that occurs around the fossil shells as shown in Fig. 2B for a sample of Facies 1, it can be found around the fossil shells (Fig. 2H) in Facies 2. In comparison with Facies 1 and 2, the radial cementation can be found in a much

Table 1
Petrophysical parameters sorted by minimum, maximum and mean values with standard deviation for all studied carbonate samples (26 samples represent *MFA-1*, while 8 samples represent *MFA-2* and 8 samples represent *MFA-3*).

Parameter	All Carbonate Samples			
	Min	Max	Mean	Std. Dev.
σ_g [g/cm^3]	2.68	2.8	2.701	0.019
σ_b [g/cm^3]	2.324	2.64	2.507	0.074
ϕ	0.022	0.17	0.072	0.031
k [mD]	0.0002	900	26.3	140
$\boldsymbol{\rho}$ [Ωm]	5.28	121	32.2	22.2
v_p [m/s]	5270	6246	5807	245
k_H [mD]	0.002	900	51.4	197
k_V [mD]	0.0002	22	1.24	4.818
$\boldsymbol{\rho_H}$ [Ωm]	5.28	102	27	19.4
$\boldsymbol{\rho_v}$ [Ωm]	13.5	121	37.5	24
v_{pH} [m/s]	5270	6117	5755	255
v_{pV} [m/s]	5510	6246	5857	230

Table 2
Petrophysical parameters sorted by minimum, maximum and mean values with standard deviation for each facies.

Parameter	*MFA-1*				*MFA-2*				*MFA-3*			
	Min	Max	Mean	Std. Dev.	Min	Max	Mean	Std. Dev.	Min	Max	Mean	Std. Dev.
σ_g [g/cm^3]	2.68	2.71	2.7	0.007	2.7	2.8	2.72	0.03	2.68	2.71	2.7	0.009
σ_b [g/cm^3]	2.41	2.62	2.53	0.05	2.32	2.49	2.4	0.06	2.46	2.64	2.53	0.06
ϕ	0.029	0.105	0.06	0.018	0.087	0.17	0.119	0.029	0.022	0.091	0.063	0.024
k [mD]	0.0002	0.26	0.04	0.07	0.03	900	138.16	312.18	0.001	0.04	0.01	0.01
$\boldsymbol{\rho}$ [Ωm]	17.73	61.34	32.41	12.18	5.28	17.89	13	4.83	17.57	121	50.96	38.88
v_p [m/s]	5390	6170	5849	206	5270	6077	5609	262	5430	6246	5848	291
k_H [mD]	0.007	0.263	0.064	0.081	5.488	900	269.9	425.461	0.002	0.039	0.017	0.016
k_V [mD]	0.0002	0.173	0.024	0.047	0.028	22	6.43	10.505	0.001	0.012	0.004	0.005
$\boldsymbol{\rho_H}$ [Ωm]	17.73	36.75	26.77	6.17	5.28	14.66	9.43	4	17.57	102.35	45.37	38.524
$\boldsymbol{\rho_v}$ [Ωm]	19.83	61.34	38.05	14.22	13.51	17.89	16.58	2.08	25.94	121	56.56	44.27
V_{pH} [m/s]	5390	6117	5819	200	5270	6077	5578	436	5430	6013	5678	258
V_{pV} [m/s]	5510	6170	5877	215	5540	5740	5631	93	5731	6246	6016	232

Where; σg is the grain density (g/cm^3); σb is the bulk density (g /cm^3);ϕ is the porosity (in fraction); k is the permeability (mD) of all the samples of each facies; ρ is the electrical resistivities (Ωm) of all the samples of each facies at concentration 60,000 ppm,; v_p is the compressional wave velocity (P-wave, m/s) of all the samples of each facies; k_H is the horizontal permeability; k_V is the vertical permeability; ρ_h is the horizontal electrical resistivity; ρ_v is the vertical electrical resistivity; v_{pH} is the horizontal P-wave velocity; v_{pV} is the vertical P-wave velocity.

Table 3
Compilation of anisotropy coefficients for all studied carbonate samples sorted by minimum, maximum and mean values with standard deviation for all studied carbonate samples.

Coefficient of Anisotropy	Min	Max	Mean	Std. Dev.
$A_k = (k_H/k_V)$	1	3.74	1.83	0.79
$A_\rho = (\rho_v/\rho_h)^{1/2}$	0.8	3.39	1.52	0.59
$Av = V_{pH}/V_{pV}$	0.93	1.07	0.98	0.04

the lower extent in Facies 3. Glauconite grains generally occur in the typical 'popcorn shape' as described by Triplehorn (1966) [23] and McRae (1972) [14]. In Facies 1 the quantification of glauconite content by color differentiation resulted in about 0.8%. In Facies 2, the amount of glauconite is relatively high with a measured average amount of about 6.8%, (Fig. 2F and G). In Facies 3, most of the micritic matrix and glauconite grains can be found within fossil shells (Fig. 2I–L), the glauconite content is with about 6.8% almost equal to Facies 2. The iron oxides minerals can only be found in Facies 3. The fossil traps also contain a visually estimated total amount of about 5–10% iron minerals (Fig. 2K and L). The porosity may be due to the dissolution of shell fragments (Fig. 2C), and results completely from moldic and oomoldic pores as shown in Fig. 2D. Although some of the moldic pore spaces in the Facies 1 are filled with diagenetic dolomite in the Facies 2, the porosity of Facies 2 is higher than for Facies 1 and 3. The porosity due to the dissolution of brachiopod fragments is present in Fig. 2E. May be due to the high amount of cementation by iron oxides and only few moldic pores, the porosity in Facies 3 is low.

3.2. Petrophysical investigations

The grain density shows reasonable values, as all of the samples are limestones. The resulting values closely compare to the grain density of calcite with 2.71 g/cm^3 [16], where the averaging value of grain density is 2.70 g/cm^3. The grain density ranges from 2.68

Table 4
Compilation of anisotropy coefficients for each facies sorted by minimum, maximum and mean values with standard deviation for each facies.

Coefficient of Anisotropy	*MFA-1*				*MFA-2*				*MFA-3*			
	Min	Max	Mean	Std. Dev.	Min	Max	Mean	Std. Dev.	Min	Max	Mean	Std. Dev.
$A_k = (k_H/k_V)$	1.06	3.08	1.55	0.55	2.53	3.74	3.04	0.59	1	2.03	1.54	0.46
$A_\rho = (\rho_v/\rho_H)^{1/2}$	0.99	2.32	1.41	0.4	1.16	3.39	2.05	1.03	0.8	1.73	1.34	0.44
$Av = V_{pH}/V_{pV}$	0.95	1.07	0.99	0.04	0.93	1.06	0.99	0.07	0.93	0.96	0.94	0.02

Where; A_k is the permeability coefficient of anisotropy, A_ρ is the electrical coefficient of anisotropy, A_v is the seismic anisotropy ratio (P-wave coefficient of anisotropy).

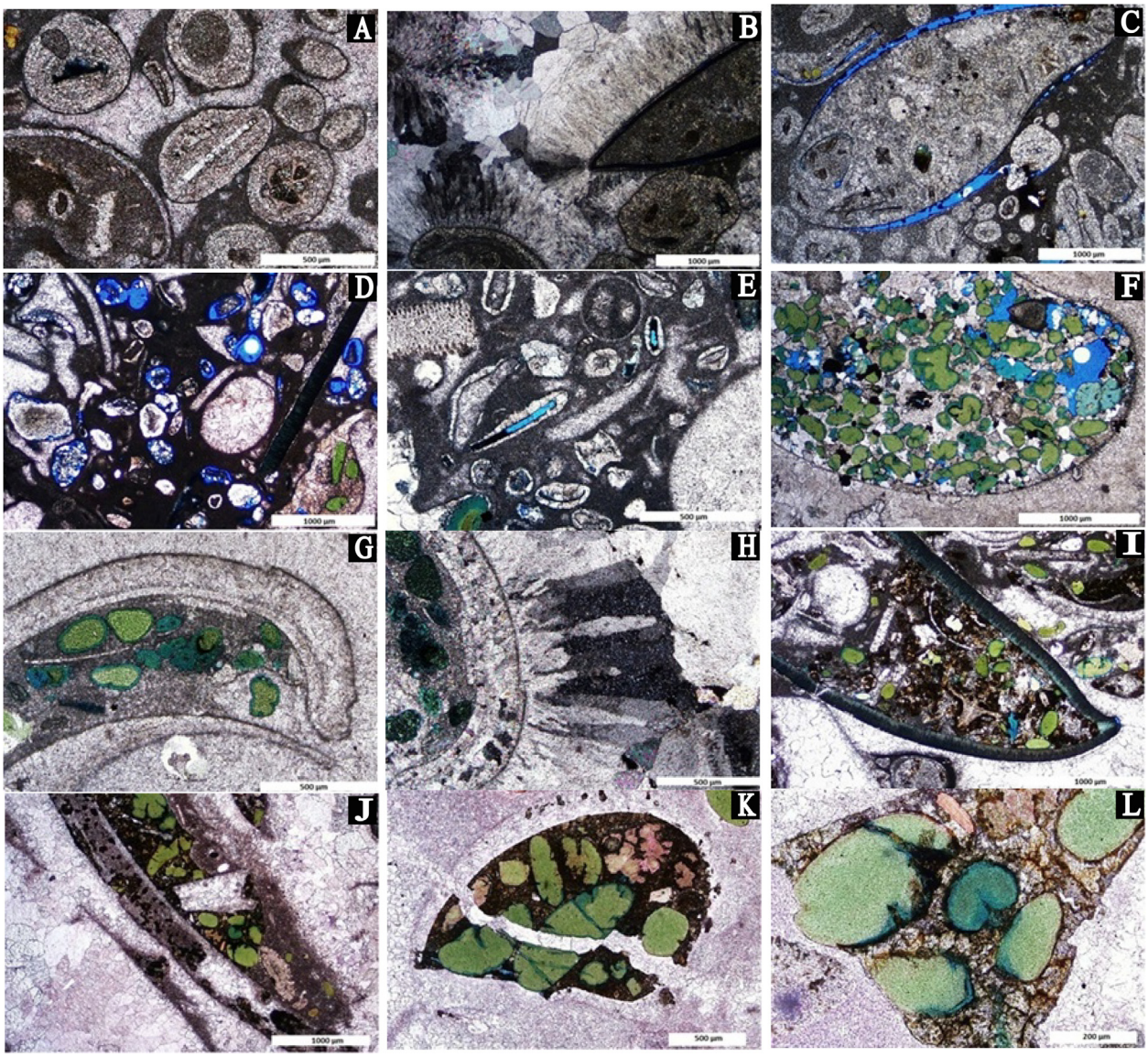

Fig. 2. Ooid grains with biomorphs, bioclasts and sometimes already dissolved shell fragments (A), (sample M1-1, 4x, PPL), *MFA-1*. Radial cementation around the shell fragments and sparitic cementation in the bigger pore spaces (B), (sample M1-1, 2x, XPL), *MFA-1*. Moldic pore space due to dissolved fossil shell (C), (sample M1-1, 2x, PPL), *MFA-1* and Oomoldic porosity (D), (sample M1-1, 2x, PPL), *MFA-1*. Ooid grains with dissolved brachiopod fragments in the center (E), (sample P1, 4x, PPL), *MFA-2*. Typical fossil trap of a gastropod shell filled with glauconite grains (F and G) (sample P3, 2x, PPL and sample P3, 4x, PPL, respectively), *MFA-2* and radial cementation around a fossil shell (H), (sample P3, 4x, XLP), *MFA-2*. Moldic pore and fossil trap structure with glauconite and iron minerals inside, calcitic sparite cement outside the trap (I and J), (sample P3, 2x, PPL and P8, 2x, PPL, respectively), *MFA-3* and glauconite, micrite and iron minerals in the fossil trap and sparry calcite cements outside (K and L), (sample P8, 4x, PPL and P8, 10x, PPL, respectively), *MFA-3*.

to 2.80 g/cm^3, the minimum grain density refers to limestone and the maximum grain density refers to the presence of dolomite [13]. The bulk density is lower than the grain density, because of the normally lighter density of the pore filling compared to the density of the grains. Averaging all bulk density values yields a mean density of 2.51 g/cm^3.

In the geological studies, porosity generally originates from depositional processes (primary porosity) and/or as a result of diagenetic processes (secondary porosity). Averaging all porosity (in fraction) values yields a mean porosity of 0.072. Porosity values for the studied samples spread over a relatively wide interval ranging from 0.022 to 0.170. The porosity values of *MFA-1* and of *MFA-3* are low with 0.060 and 0.063, respectively, in comparison with the porosity of *MFA-2*, which is with 0.119 much higher. Averaging all permeability values yields arithmetic mean permeability of 26.35 mD. Permeability values for the samples spread over a relatively wide interval ranging from 0.0002 mD to 900 mD. The results as compiled in Table 2 show low values of permeability for Facies 1 and 3. The average values of permeability of *MFA-1* and *MFA-3* are low with only 0.044 mD and 0.011 mD, respectively, in comparison with the permeability of *MFA-2*, which is with 138 mD much higher.

The electrical resistivity values were determined for all the studied samples of both horizontal and vertical direction. Averaging the resistivity values yields a mean resistivity of 32.25 Ωm at a concentration of the pore filling fluid of 60000 ppm, NaCl. The average values of ρ_0 for Facies 3 are much higher than of Facies 1 and Facies 2 (Table 2).

The measured velocity values of all samples vary around an average value of 5807 m/s, and spread over a relatively wide interval, ranging from 5270 to 6246 m/s. The P-wave velocity values of *MFA-1* and of *MFA-3* are slightly higher with 5849 m/s

and 5848 m/s, respectively, in comparison with the P-wave velocity of *MFA-2*, which is lower with 5609 m/s. The horizontal permeability ranges from 0.002 mD to 900 mD and reaches arithmetic mean permeability value of 51.5 mD. The vertical permeability values range from 0.0002 mD to 22 mD, with arithmetic mean permeability value of 1.24 mD.

The anisotropy of permeability values calculated from Eq. (8) of *MFA-1* and of *MFA-3* are low with 1.55 and 1.54, respectively, in comparison with the anisotropy of permeability of *MFA-2*, which is with 3.04 much higher.

The longitudinal resistivity ($\boldsymbol{\rho_H}$) ranges from 5.28 Ωm to 102 Ωm and transverse resistivity ($\boldsymbol{\rho_v}$) from 13.5 Ωm to 121 Ωm. The average transverse resistivity ($\boldsymbol{\rho_v}$) of 37.5 Ωm is significantly higher than the longitudinal resistivity ($\boldsymbol{\rho_H}$) with a value of 27.0 Ωm. The values of the coefficient of anisotropy A_ρ are low for *MFA-1* and *MFA-3* with 1.41 and 1.34, respectively, in comparison with the coefficient of anisotropy of *MFA-2*, which is with 2.05 much higher.

The vertical velocities (v_{pV}) of most of the studied carbonate samples are slightly greater than the horizontal velocities (v_{pH}). The average transverse P-wave velocity (v_{pV}) of 5857 m/s is about 1.8% higher than the longitudinal P-wave velocity (v_{pH}) of 5755 m/s. The longitudinal P-wave velocity ranges from 5270 to 6117 m/s and transversal P-wave velocity from 5510 to 6246 m/s. For most sedimentary formations $v_{pH} > v_{pV}$ is observed resulting in $A_v > 1$. The P-wave anisotropy ratios of *MFA-1* and of *MFA-2* are similar with their values ranging from 0.95 to 1.07 and from 0.93 to 1.06, respectively, while the P-wave anisotropy ratio of *MFA-3* is slightly lower, where its value is ranging from 0.93 to 0.96. Since all values of the seismic anisotropy ratio are close to one, no anisotropy is observed for the samples investigated in this study. The slight variation of horizontal and vertical P-wave velocity may be caused by using different samples for the two measurements.

The permeability values of the carbonate samples are controlled mainly by porosity and pore size [18]. In Fig. 3, the correlation between porosity and all the permeability values indicates that the permeability increases with increasing porosity. A good relationship was found between porosity and permeability, with weak to fair correlation coefficients ($R = 0.42$, 0.69 and 0.56 for *MFA*-1, *MFA*-2 and *MFA*-3, respectively). It is represented by the following power law equations:

$$\ln(k) = 2.230 * \ln(\phi) + 2.194 \text{ for } MFA - 1 \quad (11)$$

$$\ln(k) = 9.997 * \ln(\phi) + 23.496 \text{ for } MFA - 2 \quad (12)$$

$$\ln(k) = 1.608 * \ln(\phi) - 0.733 \text{ for } MFA - 3 \quad (13)$$

MFA-2 is characterized by high permeability according to the high porosity. The two other facies *MFA-1* and *MFA-3* indicate low permeability and low porosity as can be seen in Fig. 3.

The formation resistivity factor *F* has the dominant effect for permeability prediction [24]. Fig. 4 shows the formation resistivity factor that correlates well with the permeability values with fair to very good correlation coefficients ($R = 0.88$, 0.63 and 0.60 for *MFA-1*, *MFA-2* and *MFA-3*, respectively). The fitting lines can be described by the following equations:

$$\ln(k) = 18.82 - 4.122 * \ln(F) \text{ for } MFA - 1 \quad (14)$$

$$\ln(k) = 24.14 - 4.783 * \ln(F) \text{ for } MFA - 2 \quad (15)$$

$$\ln(k) = 1.932 - 1.237 * \ln(F) \text{ for } MFA - 3 \quad (16)$$

Fig. 5 shows the relationships between the directional parameters (permeability, resistivity, and P-wave velocity) in both vertical and horizontal directions of the studied carbonate samples. In Fig. 5A, the cross plot between horizontal permeability (k_H) and vertical permeability (k_V) shows that the horizontal permeability is greater than the vertical permeability. The cross plot between horizontal resistivity ($\boldsymbol{\rho_H}$) and vertical resistivity ($\boldsymbol{\rho_v}$) (Fig. 5B) shows that the values of vertical resistivity are greater than the horizontal resistivity for most of the samples. The cross plot between horizontal P-wave velocity (v_{pH}) and vertical P-wave velocity (v_{pV}) (Fig. 5C) shows that the vertical velocities of some of the studied carbonate samples are greater than the horizontal velocities, while the horizontal velocities of the other samples are greater than the vertical velocities.

Fig. 6 shows a comparison between the anisotropy of both permeability and electrical resistivity. The symbols of most samples are located close to the diagonal line that represents equal anisotropy for permeability and resistivity.

The porosity values of *MFA-1* and of *MFA-3* vary in a similar range with a maximum value of around 0.07, while *MFA-2* is characterized by a higher average porosity value, which is about 0.12. The porosity of *MFA-1* may be due to the dissolution of shell

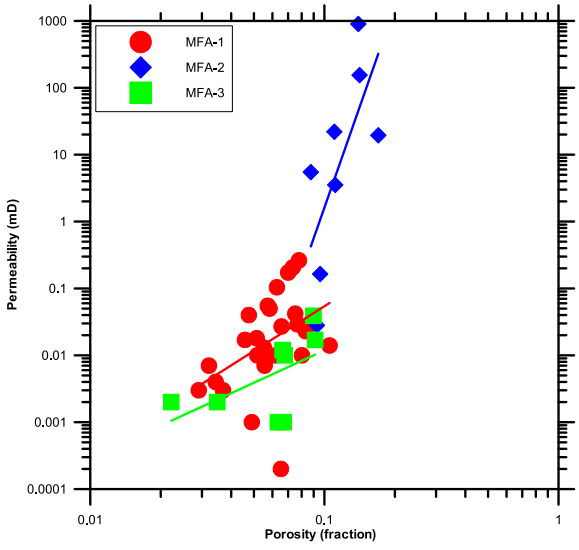

Fig. 3. Relationship between porosity and permeability of the studied samples.

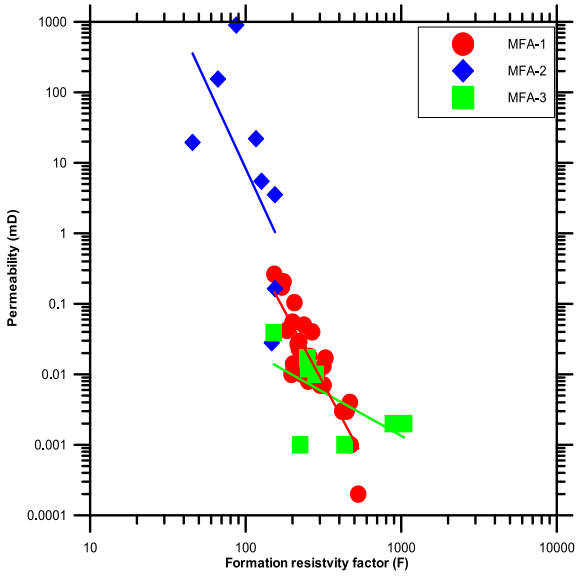

Fig. 4. Relationship between formation resistivity factor and permeability of the studied samples.

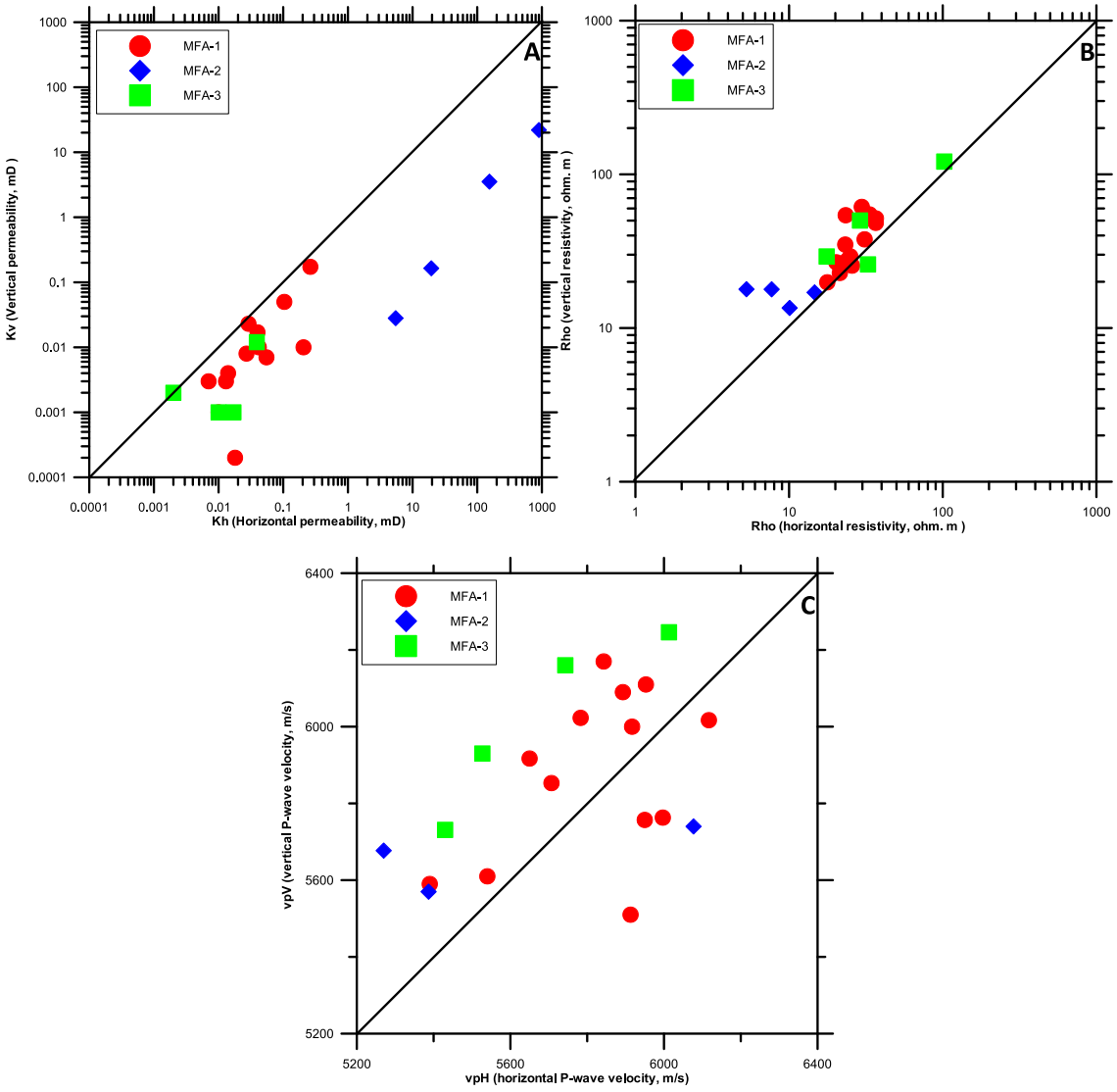

Fig. 5. The cross plots A: between horizontal permeability and vertical permeability; B: between horizontal resistivity and vertical resistivity; C: between horizontal P-wave velocity and vertical P-wave velocity of the studied samples.

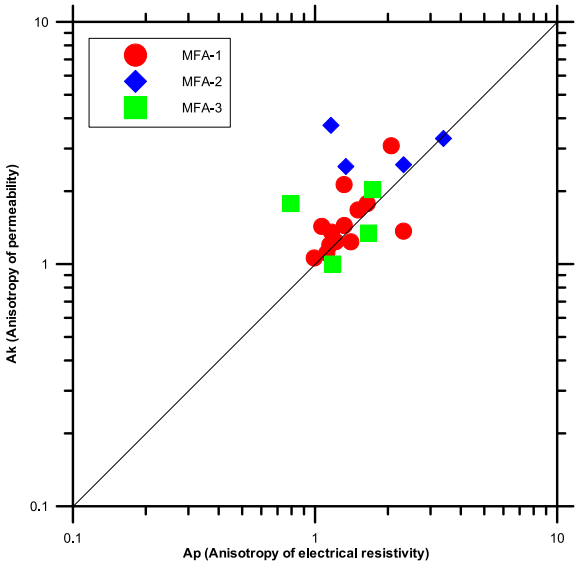

Fig. 6. The cross plot compares the anisotropy of electrical resistivity (A_ρ) and the anisotropy of permeability (A_k) of the studied samples.

fragments (Fig. 2C), and completely resulted from moldic and oomoldic pores (Fig. 2D). Although some of the moldic pore spaces are filled with diagenetic dolomite in the *MFA-2*, the porosity is higher than for *MFA-1* and of *MFA-3*. The porosity in *MFA-2* is caused by dissolved brachiopod fragments as present in Fig. 2E. The porosity in *MFA-3* is low may be due to the high amount of secondary cementation and only few moldic pores.

The high permeability of *MFA-2* is directly linked to the increased porosity in comparison to *MFA-1* and *MFA-3* (Fig. 3). The *MFA-2* exhibits a much higher porosity and permeability. The values of horizontal permeability (k_H) are mostly higher than the values of vertical permeability (k_V), where the mean value of k_H is 51.45 mD and the mean value of k_V is 1.24 mD.

The longitudinal resistivity values ($\boldsymbol{\rho}_H$) are mostly lower than the transverse resistivity values ($\boldsymbol{\rho}_v$), where the mean value of $\boldsymbol{\rho}_v$ is 37.5 Ωm and the mean value of $\boldsymbol{\rho}_H$ is 27.0 Ωm. As shown in Fig. 4, the formation factor correlates well with permeability indicating fair to very good correlation coefficients, which confirms the dominant effect of the formation factor for permeability prediction.

The coefficients of anisotropy of permeability and electrical resistivity are relatively low for the samples of *MFA-1* (1.55 and 1.41, respectively) and *MFA-3* (1.54 and 1.34, respectively), which

indicate low porosity (0.060 and 0.063, respectively). The coefficients of anisotropy of permeability and electrical resistivity remarkably increase for the samples of *MFA-2* (3.04 and 2.05, respectively), which are higher in the porosity (0.119). The higher degree of anisotropy that is observed for both resistivity and permeability for samples of *MFA-2* is caused by a better connectivity of the pore space in the horizontal direction, which corresponds to the direction in parallel to the original stratification. It should be noted that both electrical conductivity (the inverse of resistivity) and permeability are controlled by the pore space and its connectivity.

The decrease of porosity, which is observed for the samples of *MFA-1* and *MFA-3*, is mainly caused by precipitation of calcite cement or iron minerals in the pore space. The reduction in porosity is mainly accompanied by a decline in the connectivity of the pore space in horizontal direction that results in a reduced anisotropy. Using Eq. (8) as a definition for the coefficient of anisotropy for permeability as proposed by Halisch et al. (2008) [5], the resulting values become comparable with the coefficients of anisotropy for resistivity. This observation confirms that anisotropy of electrical conduction and hydraulic conduction are related to each other.

The P-wave velocity is more related to the rigidity of the grain skeleton than to the structure the pore space. The study shows that the values of transverse P-wave velocity (v_{pV}) are similar to the values of longitudinal P-wave velocity (v_{pH}). Therefore, the values of the anisotropy ratio of P-wave velocity are close to one for all facies. This means that no anisotropy can be detected in the seismic velocity for all three facies.

4. Conclusions

1. The petrographic investigations of the studied carbonates samples show three microfacies associations (*MFA-1*, *MFA-2* and *MFA-3*).
2. The grain density values indicate only a slight variation, where the resulting values closely compare to the grain density of calcite with 2.71 g/cm^3, where the averaging value of grain density is 2.70 g/cm^3.
3. The porosity and permeability for *MFA-1* and *MFA-3* are rather small, while *MFA-2* exhibits a much higher porosity and permeability.
4. Similar coefficients of anisotropy are observed for electrical resistivity and permeability.
5. A higher anisotropy in resistivity and permeability is observed for *MFA-2*, which is mainly caused by a better connectivity of the pore space in the direction in parallel to the stratification.
6. The decrease of porosity for the samples of *MFA-1* and *MFA-3* is mainly accompanied by a decline in the connectivity of the pore space in horizontal direction and a reduced anisotropy.
7. The present study confirms that anisotropy of electrical conduction and hydraulic conduction are related to each other. While the values of anisotropy ratio of P-wave velocity are close to one for all facies, this means that no anisotropy can be detected in the seismic velocity.
8. The changing glauconite content of the three microfacies has no significant effect on the petrophysical properties as well as on anisotropy.

Acknowledgements

The joint research project between the Egyptian Petroleum Research Institute, Egypt and the Institute of Geophysics at Clausthal University of Technology, Germany was supported by a grant (WE 1557/14) of the German Research Foundation, Germany (DFG). The authors would like to thank the reviewers for their great comments that helped to improve the manuscript.

References

[1] G.E. Archie, The electrical resistivity log as an aid in determining some reservoir characteristics, Trans. AIME 146 (1942) 54–62.
[2] J.B. Clavaud, A. Maineult, M. Zamora, P. Rasolofosaon, C. Schlitter, Permeability anisotropy and its relations with porous medium structure, J. Geophys. Res. 113 (2008) B01202, https://doi.org/10.1029/2007JB005004.
[3] A. El Sayed, M.A. Kassab, Y.A. El Safori, A.E. Abass, Carbonate facies and its reservoir properties, West Tushka, South Western Desert, Egypt, in: First International Conference on the Geology of the Tethys, Cairo University, 2005, pp. 267–278.
[4] R.L. Gibson, M.N. Toksöz, Permeability estimation from velocity anisotropy in fractured rock, J. Geophys. Res. 95 (1990) 15643–15655.
[5] M. Halisch, A. Weller, C. Sattler, W. Debschütz, A. El-Sayed, A complex core-log case study of an anisotropic sandstone, originating from Bahariya Formation, Abu Gharadig Basin, Egypt, Petrophysics 50 (6) (2009) 478–497.
[6] B. Issawi, Geology of Kurkur-Dungul area, Geol. Surv. Egypt 46 (1969) 102–103.
[7] M.A. Kassab, A. Weller, Porosity estimation from compressional wave velocity: a study based on Egyptian Carbonate samples, J. Earth Sci. Eng. 3 (2013) 314–321.
[8] M.A. Kassab, A. Weller, Study on P-wave and S-wave velocity in dry and wet sandstones of Tushka Region, Egypt, Egypt. J. Petrol. 24 (2015) 1–11.
[9] G.V. Keller, F.C. Frischknecht, Electrical Methods in Geophysical Prospecting, Pergamon Press, Oxford, 1966, p. 517.
[10] A.P. Koesoemadinata, G.A. McMechan, Effects of diagenetic processes on seismic velocity anisotropy in near-surface sandstone and carbonate rocks, J. Appl. Geophys. 56 (2004) 165–176.
[11] L. Louis, C. David, V. Metz, P. Robion, B. Menendez, C. Kissel, Microstructural control on the anisotropy of elastic and transport properties in undeformed sandstones, Int. J. Rock Mech. 42 (7–8) (2005) 911–923.
[12] L. Louis, T.N. Chen, C. David, P. Robion, T. Wong, S. Song, Anisotropy of magnetic susceptibility and P-wave velocity in core samples from the Taiwan Chelungpu-Fault Drilling Project (TCDP), J. Struct. Geol. 30 (2008) 948–962.
[13] G.A. McMechan, X. Zeng, Report on Lab Measurements of Electrical Properties from the Ellenburger at the Dean Word Quarry, Burnet County, Texas: Final Report, GRC Contract No. 5709-210-3889, University of Texasat Dallas, 2002.
[14] S.G. McRae, Glauconite, Earth Sci. Rev. 8 (1972) 397–440.
[15] B.S. Nabawy, Impacts of fossil anisotropy on the electric and permeability anisotropy of highly fossiliferous limestone: a case study, Mar. Geophys. Res. (2017), https://doi.org/10.1007/s11001-017-9335-2.
[16] G.R. Olhoeft, G.R. Johnson, Densities of rocks and minerals, in: Carmichael (Ed.), Practical Handbook of Physical Properties of Rocks and Minerals, Section II, CRC Press, Boca Raton Florida, 1989.
[17] Ü. Öner, Petrographical and Petrophysical Investigation on Carbonate Samples from the Tushka Area, Egypt (Master Thesis), Institute of Geophysics at Clausthal University of Technology, 2014, p. 88.
[18] Ü. Öner, A. Weller, C. Sattler, M.A. Kassab, Petrographic and petrophysical investigation on carbonate samples (Upper Cretaceous) from the Tushka Area (Egypt) with special focus on the effective pore radius, Arab. J. Geosci. 9 (2016) 229, https://doi.org/10.1007/s12517-015-2212-x.
[19] R. Said, The Geology of Egypt, Elsevier Publishing Company, Amsterdam, New York, 1962, p. 377.
[20] J. Schön, Physical Properties of Rocks: Fundamentals and Principles of Petrophysics, Elsevier, Oxford, 1996, p. 583.
[21] D. Tiab, E.C. Donaldson, Petrophysics, Theory and Practice of Measuring Reservoir Rock and Fluid Transport Properties, second ed., Gulf Publ. Co., Houston, Texas, 2004, p. 889.
[22] D. Tiab, E.C. Donaldson, Petrophysics – Theory and Practice of Measuring Reservoir Rock and Fluid Transport Properties, third ed., Elsevier Inc., Oxford, 2012, p. 950.
[23] D.M. Triplehorn, Morphology, internal structure and origin of glauconite pellets, Sedimentology 6 (1966) 247–266.
[24] A. Weller, L. Slater, A. Binley, S. Nordsiek, S. Xu, Permeability prediction based on induced polarization: insights from measurements on sandstone and unconsolidated samples spanning a wide permeability range, Geophysics 80 (2) (2015) D161–D173.
[25] O. Serra, in: Fundamentals of Well-log Interpretation: the Acquisition of Logging Data, 1988, p. 424.
[26] B. Issawi, M. El Hinnawi, M. Francis, A. Mazhar, The Phanerozoic of Egypt: Ageodynamic Approach, Geol. Surv. Egypt (1999) 1–462.
[27] R.J. Dunham, Classification of carbonate rocks according to depositional texture, AAPG Memoir 1, 1962, pp. 108–121.